Lab on a Chip

Accepted Manuscript

ROYAL SOCIETY OF CHEMISTRY

www.rsc.org/loc

Lab on a chip

RSCPublishing

COMMUNICATION

Drop transfer between superhydrophobic wells using air logic control

Cite this: DOI: 10.1039/x0xx00000x

Thach Vuong,[a] Brandon Huey-Ping Cheong,[a] So Hung Huynh,[a] Murat Muradoglu,[a] Oi Wah Liew[b] and Tuck Wah Ng[a]

Received ooth January 2012,
Accepted ooth January 2012

DOI: 10.1039/x0xx00000x

www.rsc.org/

Abstract. Superhydrophobic surfaces aid biochemical analysis by limiting sample loss. A system based on wells here tolerated tilting of up to 20° and allowed air logic transfer with evidences of mixing. Conditions for intact transfer on 15 to 60 μL drops using compressed air pressure operation were also mapped.

Droplet-based microfluidics conducted on open surfaces has been touted to offer the possibility of conducting programmable sequences of discrete steps for biochemical analysis in a far more convenient way than with continuous flow microfluidics [1, 2]. When drops are placed on flat superhydrophobic (SH) surfaces, they assume an almost spherical shape due to the dominant Cassie wetting state [3]. The relatively homogeneous evaporation of droplets on SH surfaces [4] allows for pre-concentration [5] and thus facilitates high sensitivity probing by spectroscopic and scattering techniques [6, 7]. In addition, when frozen, there is a possibility of creating samples that are highly amenable for preservation [5].

One of the advantages claimed in the use of SH surfaces is the premise of ultra-low friction [8]. Such a contention, however, is specious in the context of biochemical analysis, since movement control of the drops then presents a problem. The real merit of using such surfaces in fact lies with the low levels of sample loss due to the highly non-wetting characteristic offered. Most reported work that have applied SH surfaces appeared to seek to increase the extent of hysteresis on neighbouring hydrophobic or hydrophilic regions [9, 10], or to facilitate sample transfer towards more wetting regions [11, 12] rather than to have the drop reside on SH surface areas. While tracks allow guided transport of liquid samples along surfaces that are SH [8], the challenge remains on how to keep the sample stationary when required so that specific processes can be conducted. Using SH surface that is sticky is one option, albeit sample loss is likely [13]. It has been shown that SH semi-spherical wells allow not only liquid drops to be stably held in them but also techniques to be incorporated to deliver individual drops to them [14, 15]. To achieve lab-on-a-chip functionality, however, there is a need to move these drops between the SH wells on command. In this communication, we demonstrate this using air (or pneumatic) logic control, a scheme familiarly used in automation where compressed air is applied as the transacting medium. We devised an approach described in Fig. 1 to accomplish automated operation.

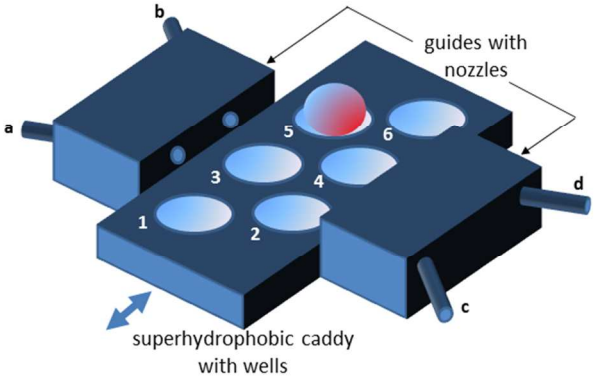

Figure 1 – Drop transfer system comprising a moveable superhydrophobic caddy with semi-spherical wells (numbered 1-6) translated between two guides with nozzles through compressed air inputs (a-d). In the position shown, delivery to inputs a, b, c, and d allow movements of drops between wells 3 to 4, 3 to 2, 4 to 5, and 4 to 3 respectively. The logical sequence of air inlet through the nozzles and location of the caddy relative to the nozzles allow full programmable control of drop transfer between the wells.

In using compressed air to cause the drop to exit the well, there is need to balance between the stability of the drop residing in the well, which can be determined by the angular extent before it exits the well given by

$$\theta = \sin^{-1}(w/2R) \quad (1)$$

where w is the width of the well and R the radius of curvature, and the ability of compressed air to cause it to exit the well. While a higher θ value imbues greater stability, displacement of the drop with air will be more difficult.

A mechanical press was used to depress a steel bearing onto a copper plate surface to create the semi-spherical wells through indentation. The indentations were then analysed using an optical profilometer (Bruker, Veeco-Wyko). In order to image the complete indentation, 35 scans (5 across by 7 down) were stitched together. Each of the single scans covered an area size of 2500µm x 1887µm. Analysis of the data was done on the Vision 64 (Ver. 5.10) software. A routine was written in Matlab to determine the mean radius of curvature of the well section. To render the copper plate superhydrophobic, it was first cleaned using absolute ethanol, allowed to air dry, and then immersed in a 24.75 mM aqueous solution of silver nitrate ($AgNO_3$) for 45 seconds to form micro and nano structures. After this, it was rinsed with copious amounts of distilled water followed by absolute ethanol before being allowed to air dry. Once dried, it was immersed in a 1 mM solution of the surface modifier $CF_3(CF_2)_7CH_2CH_2SH$ in absolute ethanol for 15 minutes. After removal, it was again rinsed with copious amounts of distilled water, followed by absolute ethanol, and then air dried. The contact angle of the surface was found to be 158°. To establish the condition of stability, drops of various sizes were placed on a well located on a manual rotary stage tilted at very slow rates. Videos of the drop on the SH surface were recorded using a high-speed camera (Fastec Troubleshooter TS1000ME) at 500 frames per second to examine the effect of compressed air delivery from a nozzle 2.54 mm in inner diameter located 10 mm from the centre of the well, on drops of various volumes located in the well. The delivery of compressed air was controlled using an electronic solenoid value was restricted to 1 second using a timer circuit patched up to interface with the solenoid valves used to allow logical switching. The pressure was measured using a digital gauge (Digitron, 2002P) when the solenoid was in the closed state. The fluorescence sample used was enhanced green fluorescent protein (EGFP) carrying a C-terminal polyhistidine tag isolated from genetically modified *Escherichia coli* and purified by immobilized metal affinity chromatography. After elution of the proteins from the chromatographic matrix, the sample was desalted into sodium phosphate buffer (pH 7.4), checked for purity by SDS-PAGE (sodium dodecyl sulfate - polyacrylamide gel electrophoresis), and quantified using the BCA (bisinchoninic acid) protein assay (Pierce). Sodium phosphate ($NaPO_4$) buffer was used to prepare a series of dilutions for the purified EGFP sample ranging from 0.065 to 1.3 µg/µL. The SH surface, before and after air puffs were blown across it was observed using an SEM (Helios Nanolab 600, FEI). To assess adhesion, a 15 µL EFGP drop was held by a tip over a glass and the SH surface for 5 minutes. They were then removed and observed using an inverted fluorescence microscope.

Based on the optical profilometry scans conducted, it was determined that R = 10 mm and w = 6.9 mm for the well created, which corresponds to θ = 20.2° using Eq. (1). From experiments conducted, it was found that θ = 19.5° ± 1.6° which on average is marginally lower than the theoretical value. This is reasonable due to the impossibility of keeping the tilt speed of the rotary stage at zero. Nevertheless, the reasonably high values denote good levels of stability offered by the wells. Practically, this infers the ability to move the SH caddy with wells containing drops from one location to another comfortably without spillage.

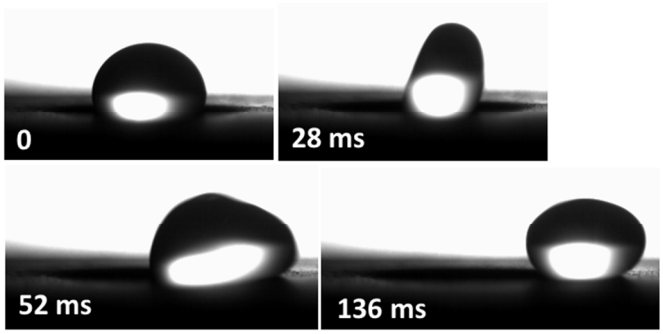

Figure 2 – Sequence of high speed images recorded at different times of using compressed air at 22.4 mBar to displace a 30 µL drop from a SH well. Despite some deformation, the drop is able to move out of the well and restore to its almost spherical shape outside the well.

From experiments conducted using compressed air delivery, it was found that the ability to successfully transfer drops out of the well is dependent on the gauge pressure. At comparatively lower air pressure applied, the drop could be transferred out of the well intact. From the high speed image sequences recorded (Fig. 2), it can be seen that the drop is able to undergo a significant degree of deformation. This can be attributed to the contour of the well which imbues added hysteresis at the front contact line. The extent of this is strong enough that the drop is able to assume an almost upright egg shape (see at 28 ms). Due to continued airflow from the left, the drop then loses its ability to maintain an upright position, resulting in a "toppling" towards the right. Interestingly a similar behaviour had been observed previously in the context of liquid delivered continuously to a drop on a SH incline [15]. Due to momentum from the airflow, the drop is able to be subsequently pushed out of the well, albeit the resistance offered by the rear contact line is relatively strong as evidenced by the significant difference in times needed to topple (28 ms to 52 ms) and to leave the well (52 ms to 136 ms). This contorting mechanism is different from the displacement of drops on flat inclines where they are able to roll as well as slide by taking advantage of the low friction air layer present between the liquid and solid phases. Naturally once the drop is able to leave the well, it will be able to restore to an energy conserving spherical form some distance ahead.

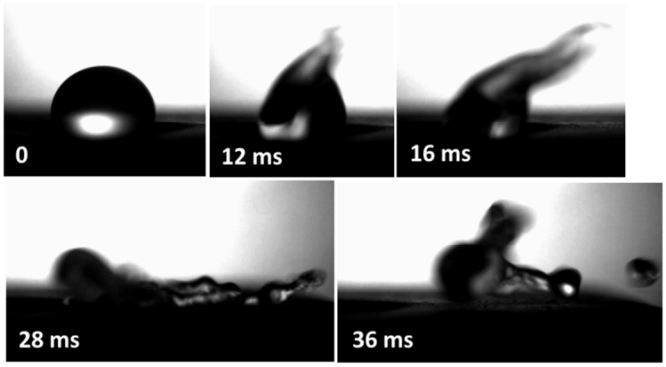

Figure 3 – Sequence of high speed images recorded at different times of using compressed air at 65 mBar to displace a 30 µL drop from a SH well. After strong deformation, the drop experienced a vibrational type of breakup that is aided by impact with the SH surface.

Under higher air pressure delivery, the drop can be seen to elongate as previously but to a much stronger extent (see at 12 ms and 16 ms

in Fig. 3). It would appear that with a more slender extension, the liquid body is able to lean more significantly to the right by harnessing the advancing angle contact hysteresis offered by the well contour. Eventually it will still "topple" over to contact the surface, although in a very energetic manner. When this happens, there is a two-fold effect on the liquid body. At its front end it is able to fragment into daughter droplets. At its rear end, it is pushed out very quickly from the well. The expeditious manner of the latter can be seen to cause a subsequent breakup into more daughter droplets.

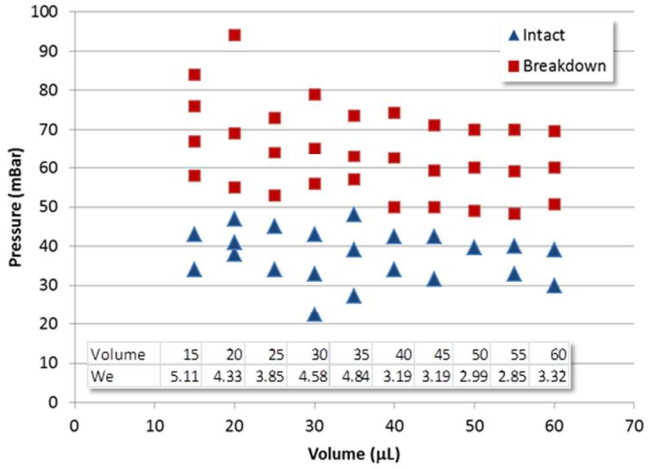

Figure 4 – Region map of breakup and intact occurrences observed of drops of various sizes actuated using compressed air at various pressures. The Weber number corresponding to breakup at various drop volumes (taken at the conditions circled) are tabulated as inset.

From an application perspective, it will be instructive to find the operational settings in which the drop transfer is able to take place sans fragmentation. The plot presented in Fig. 4 clearly indicates a capacity to do so for the range of volumes (15 µL to 60 µL) tested. It can be imputed from the plot that a single pressure setting (e.g. at 35 mBar) can be used to transfer droplets in this volume range. This facilitates the task of automating processes. The breakup of liquid droplets under an air stream has been studied previously and can appear in various distinguishable characteristics; vibrational, bag, bag-stamen, sheet striping, wave crest striping, and catastrophic [16]. They are generally taken to occur within characteristic ranges of Weber numbers [16-19] which is governed by factors ρ = air density (1.225 kg/m^3), V = droplet volume, u = air speed, σ = water surface tension (0.072 N/m), such that

$$We = \frac{u^2 \rho}{\sigma}\left(\frac{6V}{\pi}\right)^{1/3} \qquad (2)$$

In our experiments, it appeared that a vibrational type of breakup aided by impact with the SH surface was in action (see Fig. 3). In attempting to compare the Weber numbers, it is crucial to note that air is delivered here as puffs, similar to that applied in studies of tonometry [20] and olfactory response [21], rather than a steady flow. The ability to universally quantify the air velocity in puffs has not been achieved to the best of our knowledge. To do this, we devised a measurement scheme based on a dangling cantilever approach (see inset of Fig. 5) [22]. In order to simulate the force delivered to the spherical drop, a hole was created in the shield to correspond to its size (radius r = 1.52 mm to volume = 15 µL) and lined up with air delivery. Under the approximate assumption of a point load applied at the distal end of a cantilever of length L = 70 mm, width w = 5 mm, and thickness t = 0.05 mm, modulus of elasticity E = 70 GPa (aluminium), the force F can be related to the deflection δ using

$$F = \frac{Ewt^3\delta}{4L^3} \qquad (3)$$

The product of the force with the area of the hole provides measure of the air dynamic pressure such that the velocity can be determined using

$$u = \frac{1}{r}\sqrt{\frac{2F}{\pi\rho}} \qquad (4)$$

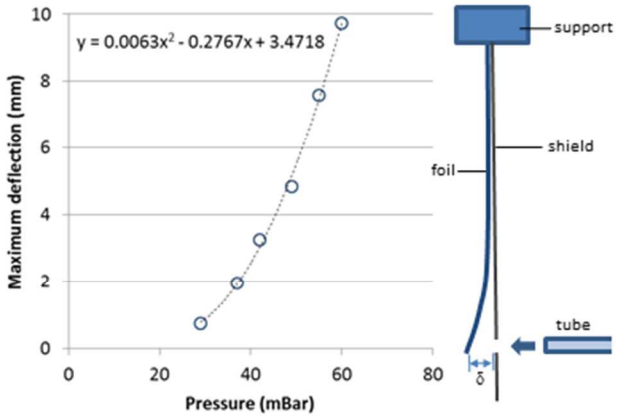

Figure 5 – Measures of maximum deflection obtained using the dangling cantilever setup depicted in the inset for various actuation air pressures applied (measured with the solenoid valve closed). Based on this, it was possible to estimate the force, dynamical pressure, and thus velocity to estimate the Weber numbers at drop breakups.

Despite the forces and thus velocities determined varying temporally during the air puff, the maximum instantaneous velocity can be taken to be that responsible for drop's breakup. The maximum deflection distribution corresponding to each pressure setting (found using high speed camera recording) is presented in Fig. 5, and can be described using a second order polynomial function. Applying the deflection values into Eqs. (2-4) gives the range of Weber number breakup values of 2.85 < We < 5.11 as tabulated in Fig. 4. They are one order smaller than that needed for a vibrational type of breakup (We < 16) [16]. We attribute this to the additional effect of the drop impacting the SH surface which will require lower inertial forces to cause the breakup. Under surface-tension-controlled vibration of the liquid body, the natural angular frequency ω is obtained by balancing the pressure due to inertial ($\sim\rho V^2/3\omega^2$) and capillary forces ($\sim\sigma/V^{1/3}$), where ρ = density, σ = surface tension, V = drop volume. Hence, $\omega \sim (\sigma/\rho V)^{1/2}$. This imputes the air blown will need to excite resonant frequencies lying in the $O(10^o)$ Hz range.

In order to illustrate the operation of the system, drops of distilled water and EGFP of 15 µL volume were deposited into separate wells (see Fig. 6a). The drop containing EGFP can be distinguished due to it giving off a bright green fluorescence under the illuminating blue LED light. Using compressed air, the drop containing EGFP was moved to coalesce with the water drop (see Fig. 5b). It has been previously shown that two drops attempting to combine on a flat SH

surface had a propensity to rebound [23] which might render the system inoperable. We did not observe such behaviour and attribute this to the well serving as a gravitational potential minimum that is able to provide additional motive for the drops to coalesce. That the combined drop was able to exhibit uniform fluorescence after only 10 seconds suggest sufficient mixing capacity caused by surface tension forces in action during coalescence of the drops [24], albeit more detailed investigations will be needed for confirmation. Through a series of compressed air supply and caddy translation operations, it was possible to quickly move the combined drop towards the opposite end of the caddy (see Fig. 6). The lack of EGFP fluorescence residue on the SH surface provides indirect indication of low sample loss on it compared with glass (see Figs. 7(a) and (b)). In addition, SEM images (see Figs. 7(c) and (d)) indicate no damage to surface microstructures due to the transfer. This is hardly surprising as the air forces used were typically in the $O(10^{-4})$ N range. The adoption of air logic is facilitated by the wide availability of air lines in many biochemistry laboratories. Even in their absence, compact and inexpensive compressors are readily available. Another advantageous point in adoption is the ready availability of connective and switching fixtures that permit simple assembly.

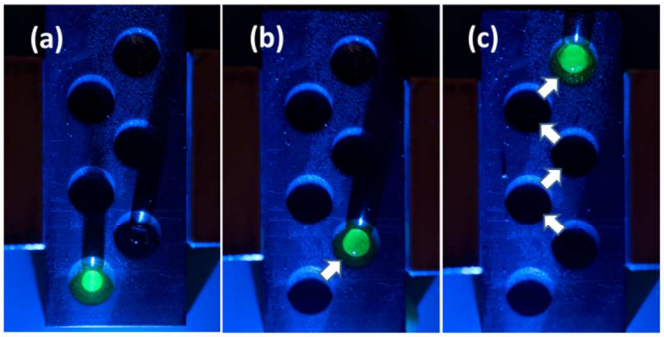

Figure 6 – Sequence of images of (a) an EGFP (which fluoresces due to LED light excitation provided from the bottom of the image) drop and water drop (poorly visible but its presence evident by the shadow that is cast) in separate wells, in which the former is moved using compressed air to coalesce with the latter (b), and then the combined drop moved sequentially to a well at one end of the caddy (c) in the system developed (path denoted by arrows).

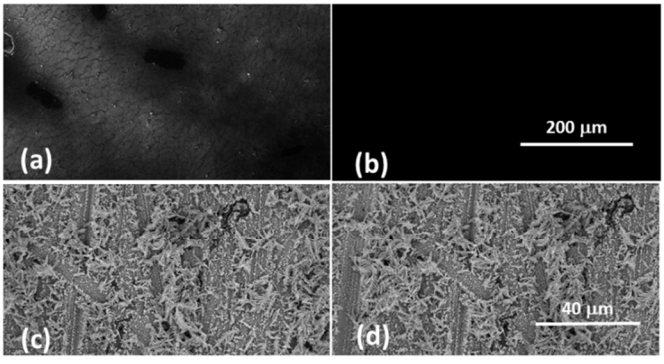

Figure 7 – Fluorescence microscopy images of after a drop containing EGFP contacted (a) glass and (b) the SH surface showed low residual protein adhesion for the latter. The almost unchanged dendritic microstructures revealed in SEM images of the SH surface (c) before and (d) after air puffs were blown across showed no damage from the transfer process.

Conclusions

An open discrete microfluidic system based on the use of a SH caddy with semi-spherical wells was developed to achieve transfer with low sample losses. Despite the known high mobility of drops on SH surfaces, the system showed good retention stability through its ability to maintain tilting extents of up to 20° before exit. A mapping exercise of the allowable transfer of drops of volumes ranging between 15 µL to 60 µL relative to the compressed air pressure applied showed regions of the drops remaining intact and of them exhibiting breakdown. It indicated a possibility of using one pressure setting to move drops in this volume range without breakdown. The breakdowns were of the vibrational type aided by impact on the SH surface. The Weber numbers corresponding to their onset were in a range of $2.85 < We < 5.11$, smaller than that found in experiments conducted with drops falling in constant velocity airflows. The capacity to transfer EGFP and water drops and with evidences of mixing was exhibited using the system.

Notes and references

[a] Laboratory for Optics and Applied Mechanics, Department of Mechanical & Aerospace Engineering, Monash University, Clayton VIC3800, Australia.

[b] Cardiovascular Research Institute, Yong Loo Lin School of Medicine, National University of Singapore, National University Health System, Centre for Translational Medicine, 14 Medical Drive, Singapore 117599.

1 D. Chatterjee, B. Hetayothin, A.R. Wheeler, D.J. King, R.L. Garrell, *Lab Chip* 2006, **6**, 199-206.
2 X. Casadevall i Solvas, A. deMello, *Chem. Commun.* 2011, **6**, 1936.
3 D. Quere, *Rep. Prog. Phys.* 2005, **68**, 2495.
4 G. McHale, S. Aqil, N.J. Shirtcliffe, M.I. Newton, H.Y. Erbil, *Langmuir* 2005, **21**, 11053.
5 F. Shao, T.W. Ng, O.W. Liew, J. Fu, T. Sridhar, *Soft Matter* 2012, **8**, 3563.
6 F. De Angelis et. al, *Nat. Photon.* 2011, **5**, 682.
7 C.A.E. Hauser et. al, *Proc. Natl. Acad. Sci. U.S.A.* 2011, **108**, 1361.
8 H. Mertaniemi et. al, *Adv. Matl.* 2011, **23**, 2911.
9 A Accardo et. al *Lab Chip* 2013, **13**, 332.
10 B. Balu, A.D. Berry, D.W. Hess, V. Breedveld, *Lab Chip* 2009, **9**, 3066.
11 S. Xing, R.S. Harake, T. Pan, *Lab Chip* 2011, 11, 3642.
12 W. Song, D. Psaltis, K.B. Crozier, *Lab Chip* 2014, **14**, 3907.
13 B. Su, S. Wang, Y. Song, L. Jiang, *Nano Res.* 2011, 4: 266.
14 T. Vuong et. al *Soft Matter* 2013, **9**, 3631.
15 M. Katariya, T.W. Ng, *J. Phy. D: Appl. Phys.* 2013, **46**, 345302.
16 M. Pilch, C.A. Erdman, *Int. J. Multiphase Flow* 1987, **13**, 741.
17 F.C. Haas, *AIChE J.* 1964, **10**, 920.
18 A.C. Merrington, E.G. Richardson, *Proc. Phys. Soc.* 1947, **59**, 1.
19 A. Wierzba, *Expt. Fluids* 1990, **9**, 59.
20 Q.K. Farhood, *Clin. Opthalmol.* 2013, **7,** 23.
21 X. Chen, Z. Xia, D.R. Storm, *J. Neurosci.* 2012, **32**, 15700.
22 T.W. Ng, Y. Panduputra *Langmuir* 2012, **28**, 453.
23 H. Mertaniemi, R. Forchheimer, O. Ikkala, R.H.A. Ras, *Adv. Matl.* 2012, **24**, 5738.
24 A.V. Anilkumar, C.P. Lee, T.G. Wang, *Phys. Fluids A* 1991, **3**, 2587.